Acta Cryst. (1974). A**30**, 639

The Effect of Disorientation on the Intensity Distribution of Non-crystalline Fibres. II. Applications

BY G. J. STUBBS

Max-Planck-Institut für medizinische Forschung, 69 Heidelberg, Jahnstrasse 29, Germany (BRD)

(*Received* 6 *August* 1973; *accepted* 15 *April* 1974)

Starting with the integral form of the correction factor derived in the previous paper [Holmes & Barrington-Leigh (1974). *Acta Cryst.* A**30**, 635–638], the explicit form of the function describing intensity in reciprocal space for slightly disoriented non-crystalline fibres is described, and simplifying approximations are made. Correction factors for real data are calculated, and the validity of the theory tested with data from tobacco mosaic virus gels. A correction factor is also given for crystalline fibres.

1. Introduction

In the previous paper, Holmes & Barrington Leigh (1974) have derived an integral allowing the intensity observed in diffraction from slightly disoriented fibres to be evaluated. However, work with tobacco mosaic virus (TMV) gels by Mandelkow (1973) has shown that a simple empirical function appears to describe the intensity, namely $A+BR$, where A and B are constants, and R is the distance from the meridian on the fibre diagram.

The present paper has two aims: to describe the form of Holmes & Barrington Leigh's function in a number of experimental situations, and to consider approximations which permit the derivation of simple correction factors to be applied to real data. These are, for slit cameras,

$$2pa/\mathrm{erf}\,(\sqrt{2}a/\alpha_0 R)$$

for point-focus cameras with significant X-ray beam size,

$$(1+2\pi p^2a^2+2\pi p^2\alpha_0^2R^2)^{1/2},$$

and for point-focus cameras with insignificant beam size

$$(1+2\pi p^2\alpha_0^2R^2)^{1/2}$$

(for explanation of symbols, see Table 1).

The second of these is quite similar to Mandelkow's empirical correction factor.

2. Evaluation of an explicit form of the intensity function

The intensity in reciprocal space is given by Holmes & Barrington Leigh as

$$I=\frac{1}{v\alpha_0^2}\int_{l=0}^{v} f(l)\exp-\left[\frac{(s-R)^2+(Z-l)^2}{2\alpha_0^2v^2}\right] i_0\left(\frac{sR}{\alpha_0^2v^2}\right)\mathrm{d}l. \quad (1)$$

These symbols and others used in this paper are explained in Table 1.

Table 1. *Symbols used in this paper*

Symbol	Meaning
I	Intensity under ideal measurement conditions
I_{calc}	Intensity in the absence of disorientation
I_{obs}	Intensity measured experimentally
α_0	Disorientation parameter
v	Distance from origin in reciprocal space
R	Distance from meridian on fibre diagram
s	Distance from meridian in transform of one particle
Z	Distance from equator on fibre diagram
l	Distance from equator in transform of one particle
Z_0	Value of Z at centre of layer line
$f(l)$	Distribution of intensity across a layer line in absence of disorientation
p	Length of coherently diffracting crystallite
P	$p^2\pi\alpha_0^2R^2$
a	Half-width of X-ray beam
i_0	$i_0(x)=I_0(x)e^{-x}$

Equation (1) is almost identical to equation (9) in the preceding paper, lacking only a factor $I_{\mathrm{calc}}(s)$ in the integrand. As $I_{\mathrm{calc}}(s)$ usually varies slowly, it has been omitted from calculations in this paper, except where its explicit form becomes important.

In this section, the form of I is described. To do this, a specific form of the function $f(l)$ is required. The usual case is a layer-line scattering function, being the squared Fourier transform of a sequence of points, of length p, separation Δp. This is

$$\sin^2(pl\pi)/\sin^2(\Delta pl\pi).$$

Near the centre (Z_0) of a layer line, this is approximated well by the Gaussian form

$$(p^2/\Delta p^2)\exp-p^2\pi(l-Z_0)^2.$$

For the following computations we have taken the form

$$f(l)=\exp-p^2\pi(l-Z_0)^2; \quad (2)$$

for the TMV particle, $p=3000$ Å (Hall, 1958; Williams & Steere, 1951).

The function I has been computed from equations (1) and (2) in the form of cross-sections in Z at fixed values of R. These are illustrated, in Fig. 1 for disorientation of $\alpha_0=2°$, at $Z_0=0{\cdot}087$ Å^{-1} (the sixth layer

line of TMV). $(\alpha_0 I)^{-1}$ as a function of R, at $Z=Z_0$, is illustrated in Fig. 2. The approximation that I is inversely proportional to R, referred to in the previous paper, is seen to be substantially improved as α_0 increases, and slightly improved as Z_0 decreases.

Fig. 3 gives the cross section in Z on the meridian for several interesting cases. Fig. 3(*a*) illustrates the cross-section for the limiting case of an infinitely long molecule [$f(l)$ is then a delta-function]. Fig. 3(*b*) and (*c*) are typical TMV cases, and Fig. 3(*d*) is the 1·5 Å reflexion of paramyosin. Asymmetry increases with increasing α_0, diffraction angle and coherent molecular length.

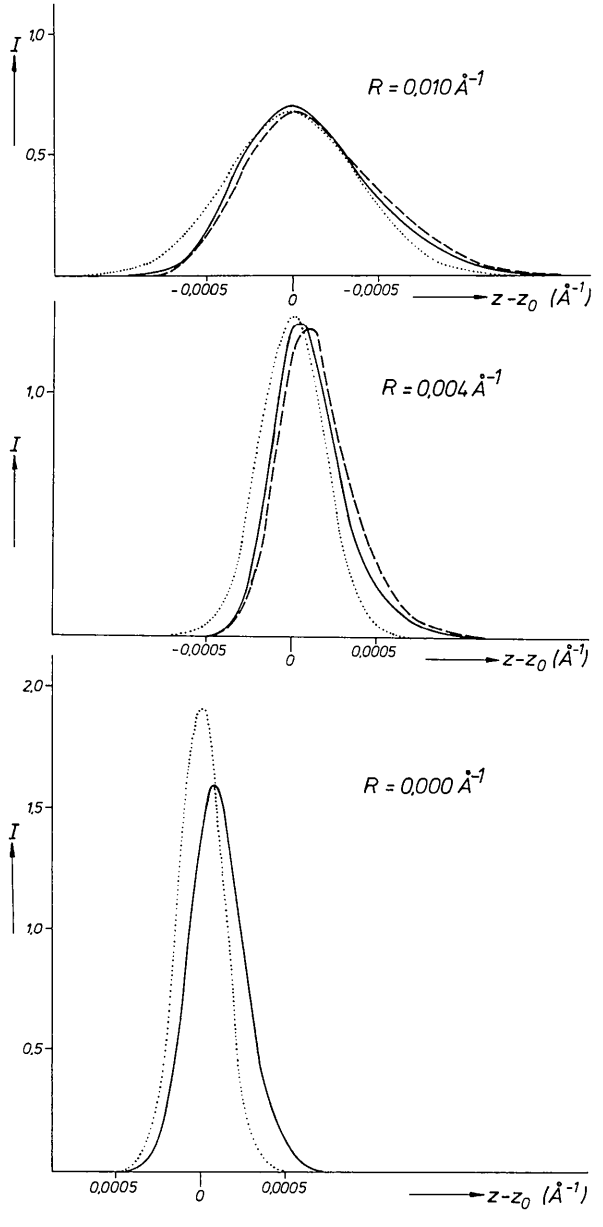

Fig. 1. Cross sections in Z of the intensity function, on a layer line with $Z_0=0{\cdot}087$ Å^{-1}. Units of intensity are arbitrary, but used consistently in Figs. 1–6. Solid lines – computed from equations (1) and (2). Broken lines – using approximation $i_0(Rs/\alpha_0^2 v^2)=\alpha_0 v/\sqrt{2\pi R}$. No cross section is given on the meridian for this approximation, as the errors become infinite. Dotted lines – calculated from equation (6).

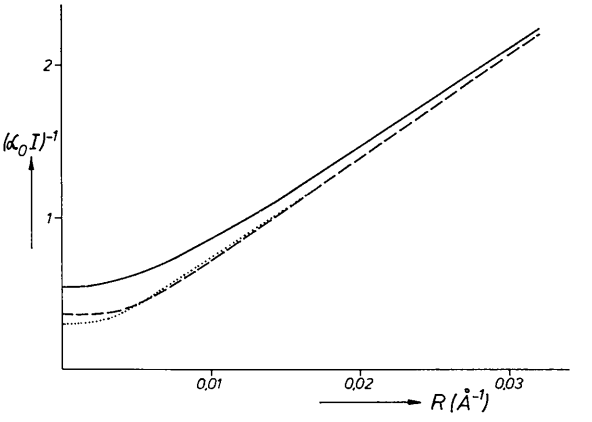

Fig. 2. $(\alpha_0 I)^{-1}$ at the centre of a layer line, as a function of R. I is calculated from equations (1) and (2). Solid line – $\alpha_0=1°$, layer line 6 for TMV; broken line – $\alpha_0=2°$, layer line 6; dotted line – $\alpha_0=2°$, layer line 3.

Fig. 3(*d*), corresponding to the 1·5 Å reflexion of paramyosin, shows that disorientation is insufficient to account for the discrepancy in the position of this reflexion, compared with that expected from a coiled-coil structure (Cohen & Holmes, 1963). This discrepancy is about 0·015 Å (Elliot, 1968). Elliot describes the reflexion as asymmetric, which probably illustrates the failure of the approximation that $I_{calc}(s)$ is constant.

3. Approximation to simplify the basic expression

(*a*) The asymptotic form $i_0(x) \to (2\pi x)^{-1/2}$ as $x \to \infty$ [Abramowitz & Stegun (1965), p. 377] may be used in equation (1) for all values of R except those very near the meridian.

(*b*) The further approximation $R=s$ should also be used in part of equation (1), so that the total approximation becomes

$$i_0(Rs/\alpha_0^2 v^2)=\alpha_0 v/\sqrt{2\pi R}\,. \qquad (3)$$

This approximation is necessary when approximation (*a*) is used. This is because, for very small s, the approximation

$$i_0(Rs/\alpha_0^2 v^2)=\alpha_0 v/\sqrt{2\pi Rs}$$

[approximation (*a*)] is not very good. Equation (3) is considerably better.

The errors caused by these two approximations are shown in Fig. 4. Although these errors are sometimes very serious, they are reduced by two further approximations, which at the same time simplify the expression for I considerably.

(*c*) It can be seen from Fig. 3 of the preceding paper that for small $\gamma-\sigma$,

$$\frac{(s-R)^2+(Z-l)^2}{v^2} \simeq \frac{(Z-l)^2}{R^2}. \qquad (4)$$

(*d*) It is assumed that the integrand in equation (1) is insignificant outside the limits of integration. This is quite reasonable except when R is very small. However, in this case it has the following further advantage:

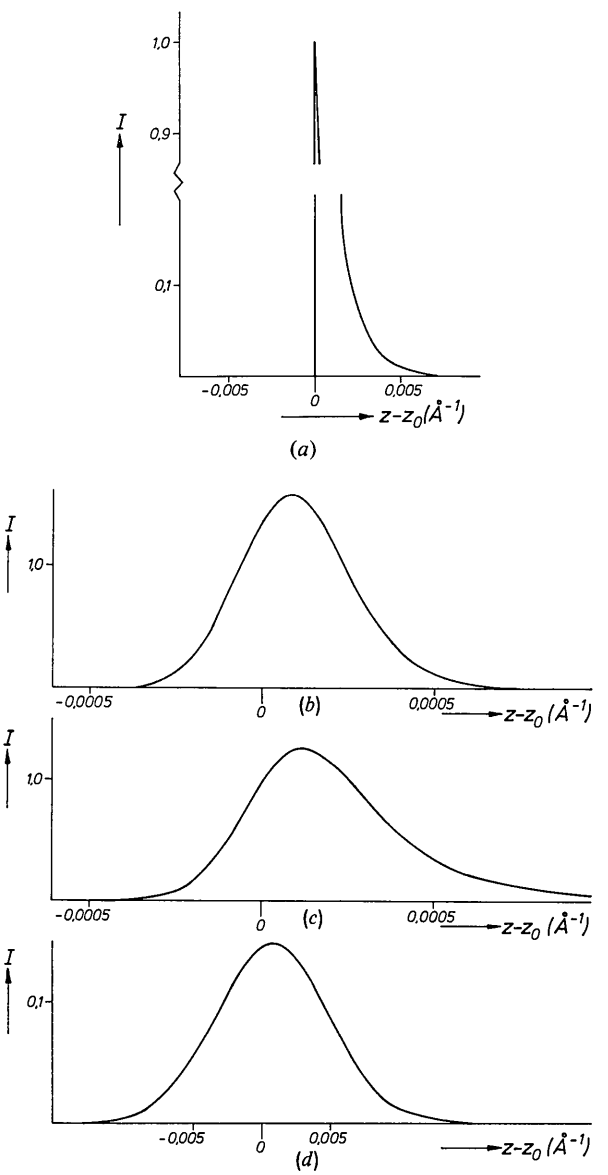

Fig. 3. Cross sections in Z of the intensity function, on the meridian, about the centre of a layer line:

	Z_0(Å^{-1})	α_0	p(Å)	Natural system
(*a*)	0·348	2°	∞	
(*b*)	0·087	2°	3000	TMV, LL6
(*c*)	0·174	2°	3000	TMV, LL12
(*d*)	0·667	2°	100	Paramyosin, 1·5 Å

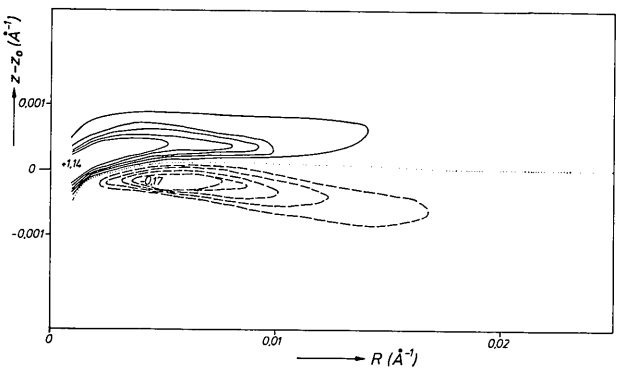

Fig. 4. Contour diagram of errors introduced into the intensity function by the approximation $i_0(Rs/\alpha_0^2v^2)=\alpha_0 v/\sqrt{2\pi R}$. Zero contour dotted; first five positive contours solid; first five negative contours broken; contour interval = 0·025, in the arbitrary units used in Fig. 1. $Z_0=0{\cdot}087$ Å^{-1}, $\alpha_0=2°$. The deepest trough and the point where the ridge crosses $R=0{\cdot}001$ Å^{-1} are marked.

The expression for I given in equation (1) is invariant with respect to R and Z_0 when integrated in Z. This is important when I is convoluted in Z with X-ray beam profiles (see below, § 4), because it causes errors in the cross section of I partly to cancel each other. The previous three approximations destroy the invariance but it is restored by this one.

We apply these four approximations and perform the integration. Let

$$P=p^2\pi\alpha_0^2R^2. \qquad (5)$$

Then

$$I=\frac{1}{\sqrt{1+2P}}\exp-\left[\frac{p^2\pi}{1+2P}(Z-Z_0)^2\right]. \qquad (6)$$

This is the main equation for diffracted intensity, from which the correction factors will be derived.*

The error introduced by using equation (6) instead of equation (1) is shown in Fig. 5 for TMV layer line 6, $\alpha_0=2°$. Comparing Fig. 4 and Fig. 5 it is clear that the last two approximations have substantially counteracted the error caused by the first two. Although the errors are still serious below about $R=0{\cdot}005$ Å^{-1}, they

* Equation (6) is very similar to equation (17) in the preceding paper. The assumption of a delta-function layer line is just equivalent to the assumption $p\gg1$ and since the coefficient of R^2 is about 10^4 for TMV (and for many other cases because shorter coherent lengths often occur with large values of α_0), the delta function is a good approximation to equation (2) for $R>0{\cdot}01$. For this domain, the intensity is proportional to R^{-1} along the middle of the layer line. Fig. 6 compares I^{-1} as computed from equations (1) and (2) with $\sqrt{2\pi p\alpha_0 R}$ and $\sqrt{1+2P}$ for layer line 6, $\alpha_0=2°$. The approximation of I^{-1} by $\sqrt{2\pi p\alpha_0 R}$ has already been discussed with reference to Fig. 2. The approximation by $\sqrt{1+2P}$ is substantially improved at lower values of α_0 (at $\alpha_0=1°$, for this layer line, the error is nowhere greater than 4%) or at lower layer-line numbers (layer line 3, $\alpha_0=2°$, has a maximum error of 10%, compared with about 25% for layer line 6).

are now very close to being antisymmetric about the centre of the layer line. This antisymmetry will reduce the errors considerably when I is convoluted in Z (see below).

The errors are illustrated in another form in Fig. 6, where cross sections of the functions whose errors are illustrated in Figs. 4 and 5 are shown together with the correct function. The partially approximated function is not shown on the meridian, where the errors become infinite.

4. The experimental correction factors

In practice I is not observed. The intensity I is convoluted with the X-ray beam cross section and the reading head of the densitometer. The latter had been found negligible in experiments varying the head size, and will not be considered further. In any case it can be thought of as a modification to the beam shape.

In the direction of R convolution has little effect except for a slight loss in resolution of $I_{\text{calc}}(s)$, since I does not change rapidly in this direction. We consider therefore only the effect of convolution in Z.

Note that the cumulative approximations illustrated in Fig. 5 have a considerably reduced effect after convolution, because the errors introduced are nearly antisymmetric, and the beam cross section is nearly symmetric, so the errors largely cancel each other. At very low R, a beam of sufficient size will effectively integrate I in Z, and there will be no residual error. This is the situation in most TMV experiments.

We consider two shapes, corresponding to the two types of beam used in TMV work (Barrett, Barrington Leigh, Holmes, Leberman, Mandelkow, von Sengbusch & Klug, 1971).

(a) X-ray beam with rectangular profile

This corresponds to the single monochromator (slit) camera. The observed intensity at the centre of the layer line

$$I_{\text{obs}}=\frac{1}{2a}\int_{Z_0-a}^{Z_0+a} I\,\mathrm{d}Z\,. \tag{7}$$

We refer to the distance $2a$ as 'effective slit size'. It depends upon the size of the X-ray beam and the geometry of the camera, being in fact the size of the image of the beam in the fibre diagram, typically about 0·01 Å^{-1} for a 14 cm specimen–film distance.

We substitute (6) in (7). The correction factor for the observed intensity I_{obs} is then seen to be

$$K=2pa/\mathrm{erf}\,\frac{2p\sqrt{\pi a}}{\sqrt{1+2P}} \tag{8}$$

(see Abramowitz & Stegun, p. 298).

If $P \gg 1$,

$$K=2pa/\mathrm{erf}\,\frac{\sqrt{2a}}{\alpha_0 R}\,. \tag{9}$$

Equations (8) and (9) give the correction factors required for slit data. Since erf (x) is almost constant for $x > 2$, correction is rarely required. This result is essentially that derived by Holmes (1959) for the zero layer line of TMV. It is valid for all layer lines.

(b) X-ray beam with Gaussian profile

This is a reasonable approximation to most point-focused beams, such as that produced by the double monochromator used by Barrett *et al.* (1971).

The beam intensity is

$$I_{\text{beam}}=\frac{1}{a\sqrt{2\pi}}\exp\left(-Z^2/2a^2\right). \tag{10}$$

Convolution of (10) and (6) gives

$$I_{\text{obs}}=\frac{1}{a\sqrt{1+2P}}\times\int_{-\infty}^{\infty}\exp-\left[(Z-Z_0)^2\left(\frac{1}{2a^2}+\frac{p^2\pi}{1+2P}\right)\right]\mathrm{d}z\,.$$

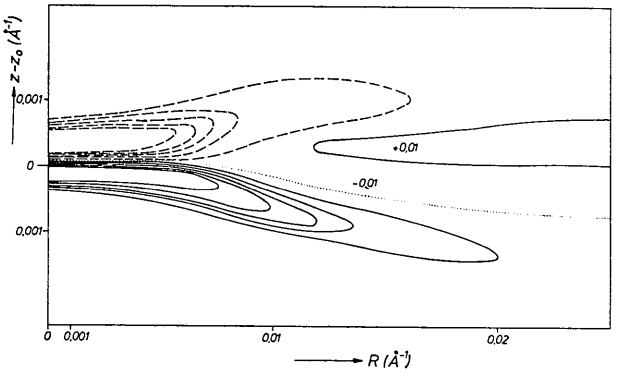

Fig. 5. Contour diagram of the errors introduced into the intensity function in equation (6). Non-meridional extremes are marked. Parameters are the same as in Fig. 4.

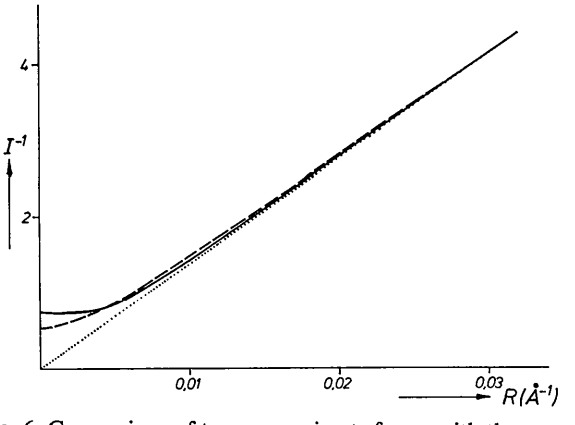

Fig. 6. Comparison of two approximate forms with the correct intensity function, on the centre of TMV layer line 6, for $\alpha_0=2°$. Solid line – the reciprocal intensity function; long dashes – $\sqrt{1+2P}$; short dashes – $\sqrt{2\pi p\alpha_0 R}$.

Evaluation of the integral leads to the required correction factor:

$$K=(A+BR^2)^{1/2} \qquad (11)$$

where

$$A=1+2\pi p^2a^2$$

and

$$B=2\pi\alpha_0^2p^2.$$

This is the correction factor for point-focused data.

The delta function approximation to $f(l)$ used by Holmes & Barrington Leigh is equivalent to omitting the 1 from A, and is usually valid over the whole domain of R, in contrast to equation (6). It is evident that R dependence is preserved for large R in both (9) and (11).

5. Experimental tests

Two sets of experimental data from TMV were made available by Dr E. Mandelkow, one from a point-focus camera and one from a slit camera. In each case, data was obtained by scanning along the centre of layer lines and corrected for all factors except disorientation in the manner described by Barrington Leigh (1970).

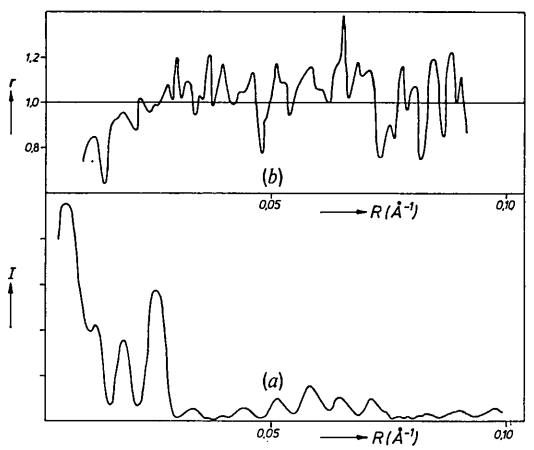

Fig. 7. The third layer line of the transform of TMV (*a*) and the ratios of simulated to observed intensities (*b*).

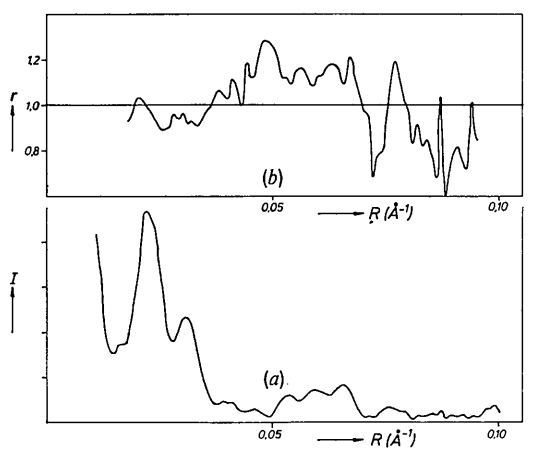

Fig. 8. The sixth layer line of the transform of TMV (*a*), and the ratios of simulated to observed intensities (*b*).

The correction factor for slit data was given in equation (8). Erf (x) is effectively (within 1 %) constant for $x > 2$, so over the domain used ($R<0{\cdot}1$) the slit data would not require correction. Error is introduced at low values of R, because the approximation that I_{calc} is constant is not sufficiently accurate for evaluating the integral in equation (7). However, it was assumed that for the larger part of the layer lines examined, slit data contained no systematic deviations from the square of the transform. Such deviations would be caused by large and rapid fluctuations in I_{calc}. These occur in the TMV data, but only for $R < 0{\cdot}03$.

Subject to disorientation correction, point-focus data should be accurate on a much larger part of the layer line. However, it is difficult to estimate accurately the quantities a and α_0 needed for such a correction. The procedure adopted, therefore, was to compare point-focus with slit data, and determine the values of $\alpha_0/\sqrt{1/2\pi+p^2a^2}$ and a scale factor by least-squares fitting of equation (11) for $0{\cdot}03 < R < 0{\cdot}10$.

The whole of the layer line was then corrected by applying equation (11) to the point-focus data. The effect of disorientation was calculated by applying equation (7) numerically, but including $I_{calc}(s)$, to simulate slit data. This was then compared with the observed slit data.

6. Experimental results

Two layer lines, the third and sixth, were used. (These are the only layer lines which provide near-meridional data.) Table 2 gives the least-squares parameters and standard deviations obtained from equation (11). These are consistent with values of 1° for α_0 and $\sim 100\mu$m for the X-ray beam focal width which are in reasonable agreement with expected values. High accuracy is not available by this method, since only the points nearest the meridian have very much influence on the quantity a.

Table 2. *Least-squares parameters and standard deviations obtained by fitting TMV data to the equation* $I_{obs}=(A+BR^2)^{-1/2}$

Layer line	A	B	S.D. in I_{obs}
3	0·39	260	0·32
6	0·54	245	0·61

Figs. 7(*b*) and 8(*b*) show the ratios of simulated slit intensities to observed intensities, as a function of R. They are shown as continuous data to facilitate comparison with Figs. 7(*a*) and 8(*a*) which show the corrected point-focus measured intensities (the best representation of the square of the transform available).

It is clear that the only systematic error is a tendency for the ratios to follow the measured intensities, particularly on the third layer line at low R. This is attributed to the fact that even point-focus data is somewhat averaged by the X-ray spot.

When allowance is made for this source of error, it is clear that Figs. 7(*b*) and 8(*b*) confirm the validity of equation (11) under the conditions studied.

7. Previously derived correction factors

Several authors have derived correction factors for disorientation of fibres. Probably the best known is that of Franklin & Gosling (1953). Their correction factor is shown below (§ 8) to be a special case of a more general form of equation (6).

Rather than correct a point measurement of intensity, some authors, for example Langridge, Wilson, Hooper, Wilkins & Hamilton (1960), have made measurements by integrating arcs, either radially or circumferentially. It is a simple procedure to show that the correction factors are then approximately v and $1/v$ respectively. The radial integration correction factor is the same as that given by Franklin & Gosling, but in this case is reasonably accurate for a wide range of situations.

Fraser, MacRae, Parry & Suzuki (1971) derived a correction factor from similar premises to Holmes & Barrington Leigh, but using a square-wave function for layer-line cross section and particle distribution. Their correction factor has the same dependence upon $(p\alpha_0 R)^{-1}$ at high values of R, as may be shown by applying the approximation

$$\cos \delta_0 = 1 - \delta_0^2/2$$

to their final equations (δ_0 is roughly equivalent to our α_0). However, part of their derivation assumed thin layer lines, and because of this, their expression breaks down near the meridian.

8. Modifications required for crystalline fibres

Subject to the approximation limits described above, the corrections given are generally applicable to intensities from non-crystalline disoriented fibres. When crystallinity is present, the approximation that $I_{\text{calc}}(s)$ varies slowly may no longer be valid. In this case, $I_{\text{calc}}(s)$ must be included in the integral in equation (1), and equation (6) rederived. For a crystalline fibre we may consider $I_{\text{calc}}(s)$ Gaussian, and write

$$I_{\text{calc}}(s) = \exp -q^2\pi(s-R_0)^2$$

where q is the thickness of a crystallite. By applying the approximations from § 3, we again reach equation (6), but this time P [see equation (5)] has a different form, namely

$$P = [(p-q)^2 + q^2 v/R_0^2]\pi\alpha_0^2 R^2.$$

In the special case when $p=q$, equation (6) shows on the centre of the layer line a dependence upon v^{-1} instead of R^{-1}. This is the dependence found by Franklin & Gosling (1953), since $p=q$ implies that all disorientation arcs are of constant width in the direction of v, an assumption inherent in their treatment. However, for most crystalline fibres, $p \gg q$, and the correction for non-crystalline fibres applies.

9. Conclusion

The main result derived in this paper is equation (11), which gives the correction factor for disorientation to be applied to data collected using a point-focused beam. If the beam size is substantially larger than the natural layer-line thickness (in practice by more than a factor of two or three), this factor is accurate over the whole fibre diagram.

In the other extreme case, of a vanishingly small X-ray beam or a very thick layer line, equation (11) reduces to equation (6). The validity of this correction factor depends upon R and α_0, and to a lesser degree upon Z. Fig. 9 summarizes the regions of the fibre diagram in which equation (6) gives the correction factor to within 1% and 5%, for $\alpha_0 = 1°$, 2° and 5°.

For cases between these two extremes equation (11) may be used, with accuracy judged from the extreme cases. Near the meridian, unless the X-ray beam is large, the full form [equation (1)] must be used.

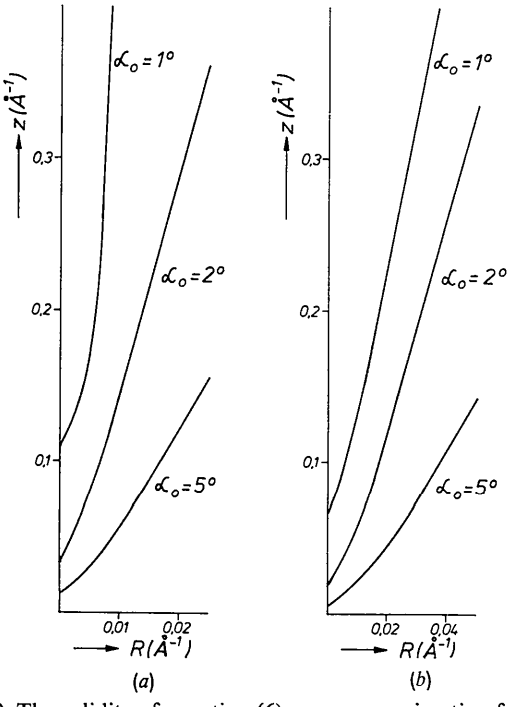

Fig. 9. The validity of equation (6) as an approximation for the intensity function, for various degrees of disorientation. Each diagram represents the fibre diagram. For a given disorientation, the equation is correct in all regions to the right of the line marked with that disorientation, to within 5% (*a*) or 1% (*b*).

I would like to thank Professor K.C. Holmes and Dr J. Barrington Leigh for helpful discussions, and Mrs G. Eulefeld for her assistance with the diagrams. I am particularly grateful to Dr E. Mandelkow, who provided the TMV data, and generously made available his own results.

References

ABRAMOWITZ, M. & STEGUN, I. A. (1965). *Handbook of Mathematical Functions*. New York: Dover.

BARRETT, A, N,. BARRINGTON LEIGH, J., HOLMES, K. C., LEBERMAN, R., MANDELKOW, E., VON SENGBUSCH, P., & KLUG, A. (1971). *Cold Spring Harbor Symp. Quant. Biol.* **36**, 433–448.

BARRINGTON LEIGH, J. (1970). *Method for the X-ray diffraction Analysis of a Helical Virus*. Thesis, Univ. of Cambridge.

COHEN, C. & HOLMES, K. C. (1963). *J. Mol. Biol.* **6**, 423–432.

ELLIOT, A. (1968). *Symposium on Fibrous Proteins*, Edited by W. G. CREWTHER. Sydney: Butterworths.

FRANKLIN, R. E. & GOSLING, R. G. (1953). *Acta Cryst.* **6**, 678–685.

FRASER, R. D. B., MACRAE, T. P., PARRY, D. A. D. & SUZUKI, E. (1971). *Polymer*, **12**, 35–56.

HALL, C. E. (1958). *J. Amer. Chem. Soc.* **80**, 2556–2557.

HOLMES, K. C. (1959). *X-ray Diffraction Studies on Tobacco Mosaic Virus and Related Substances*. Thesis, Univ. of London.

HOLMES, K. C. & BARRINGTON LEIGH, J. (1974). *Acta Cryst.* A**30**, 635–638.

LANGRIDGE, R., WILSON, H. R., HOOPER, C. W., WILKINS, M. H. F., & HAMILTON, L. D. (1960). *J. Mol. Biol.* **2**, 19–37.

MANDELKOW, E. (1973). *Röntgenstrukturuntersuchung am Tabakmosaicvirus*. Thesis, Univ. of Heidelberg.

WILLIAMS, R. C. & STEERE, R. L. (1951). *J. Amer. Chem. Soc.* **73**, 2057–2061.

Acta Cryst. (1974). A**30**, 645

Morphologie et Propriétés Optiques des Cristaux de Lysozyme de Poule de Type Quadratique et Orthorhombique

PAR BERNARD CERVELLE, FABIEN CESBRON ET JEAN BERTHOU

Laboratoire de Minéralogie-Cristallographie, associé au CNRS, Université de Paris VI, Tour 16, 4 *place Jussieu*, 75230 *Paris Cédex* 05, *France*

ET PIERRE JOLLÉS

Laboratoire de Biochimie, Université de Paris VI, 96 *boulevard Raspail*, 75272 *Paris Cédex* 06, *France*

(*Reçu le* 12 *mars* 1974, *accepté le* 10 *avril* 1974)

Large crystals of hen egg-white (HEW) lysozyme, both tetragonal and orthorhombic, have been studied with a goniometer and optical methods. As the crystals are particularly stable, some of their optical properties have been measured, mainly the refractive indices determined from reflectance measurements under a photometric microscope. Orthorhombic HEW lysozyme: crystals show the faces (010), (011) and (110). Refractive indices $n_{[001]}=n_g=1{\cdot}562$ to $1{\cdot}547$ ($\lambda=480$–640 nm); $n_{[100]}=n_m=1{\cdot}560$ to $1{\cdot}544$; $n_{[010]}=n_p=1{\cdot}550$ to $1{\cdot}532$. Maximum birefringence $0{\cdot}013$ ($\lambda=589$ nm). Optic axial angle $2V=48$ to 51°. Tetragonal HEW lysozyme: crystals formed by the association of a tetragonal {110} prism and a {101} tetragonal bipyramid. Refractive indices $n_{[001]}=n_e$ and $n_{[100]}=n_o$, with an aging phenomenon in these crystals, n_e varying between $1{\cdot}580$ and $1{\cdot}545$, n_o between $1{\cdot}575$ and $1{\cdot}538$ ($\lambda=589$ nm). Maximum birefringence $0{\cdot}007$. HEW lysozyme crystals are examples of good-quality protein crystals. Their refractive indices are surprisingly high for organic substances.

Introduction

L'obtention de cristaux de protéines de dimensions millimétriques rend possible, en principe, l'étude de leurs propriétés optiques. Peu d'études ont été consacrées à ces problèmes depuis celles que Perutz, Bragg & Pippard ont faites en 1953 sur des cristaux d'hémoglobine. Ceci s'explique par le fait que le cristallographe vise essentiellement à la connaissance de la structure moléculaire de la protéine et non à celle des propriétés physiques du cristal, et d'autre part parce qu'une telle étude présente de nombreuses difficultés. La plupart des cristaux de protéine sont très sensibles à toute variation du milieu de cristallisation et ne supportent d'en être séparés qu'un court laps de temps. Beaucoup d'autres sont instables dans le temps et passent à l'état amorphe plus ou moins rapidement.

Le cas qui été choisi dans cette étude, les cristaux de lysozyme de blanc d'oeuf de poule (EC 3.2.1.17), était intéressant à plus d'un titre. D'une part la structure cristalline de lysozyme a été déterminée (Blake, Mair, North, Phillips & Sarma, 1967) à partir de cristaux quadratiques, appelés dans cette étude cristaux de type *A*. D'autre part, une deuxième forme cristal-